Ecological Modelling 256 (2013) 16–22

Contents lists available at SciVerse ScienceDirect

Ecological Modelling

journal homepage: www.elsevier.com/locate/ecolmodel

Sensitivity of euphotic zone properties to CDOM variations in marine ecosystem models

Agurtzane Urtizberea [1], Nicolas Dupont [2], Rune Rosland, Dag L. Aksnes *

Department of Biology, University of Bergen, 5020 Bergen, Norway

ARTICLE INFO

Article history:
Received 22 November 2012
Received in revised form 13 February 2013
Accepted 14 February 2013

Keywords:
CDOM
Light attenuation
Euphotic zone
Eutrophication
Ecosystem model
Nutricline depth

ABSTRACT

In marine ecosystem models, the underwater light intensity is commonly characterized by the shading of phytoplankton in addition to a background light attenuation coefficient. Colour dissolved organic matter (CDOM) is an important component of the background light attenuation, and we investigate how variation in CDOM attenuation affects euphotic zone properties in a general marine ecosystem model. Our results suggest that euphotic zone properties are highly sensitive to CDOM variations occurring in nature. While the nutrient input to the euphotic zone scales the magnitude of the primary production, the vertical structure of nutrients and phytoplankton is largely determined by the variation in CDOM attenuation in our simulations. This suggests that knowledge of CDOM variation is useful to constrain uncertainties in predictions of water column structure in marine ecosystem modelling, but also in analyses utilizing the oceanic nutricline depth as proxy for primary production. Finally, according to our sensitivity analysis, many coastal areas experiencing high loads of terrestrial CDOM are expected to show eutrophication symptoms induced by altered optics.

1. Introduction

In traditional marine ecosystem modelling (e.g. Radach and Maier-Reimer, 1975; Fasham et al., 1990; Huisman et al., 2006) it is common to define a system of partial differential equations representing state variable such as nutrients, phytoplankton, and zooplankton (NPZ models) as a function of space (1-3D) and time. This prognostic approach has also been extended to include many functional organism groups (Follows et al., 2007) as well as several trophic levels such as in end-to-end models (Travers et al., 2007). In such models light and nutrients are limiting factors for the primary production. While nutrients provide mass for production, light feeds primary producers with the energy required for photosynthesis. Light energy is often approximated by a quantity termed the photosynthetic active radiation (PAR) which is the amount of energy or photons that are summed over the range of wavelengths utilized in photosynthesis (Kirk, 2011). The fraction (f_z) of the surface PAR that penetrates to a depth (z) is commonly specified according to $f_z = e^{-Kz}$ where the total attenuation coefficient for downwelling PAR (K, m^{-1}) is $K = K_w + k_pP + K_x$. The three terms represent attenuation due to clear water (K_w), to phytoplankton biomass (k_pP, where P is the phytoplankton concentration and k_p the specific attenuation coefficient), and to other particulate and dissolved matter (K_x). Bricaud and Stramski (1990) noted that models of primary production could be refined by using archives of geographical observations of non-algal (i.e. K_x) light absorption coefficients. This is used to estimate phytoplankton biomass (i.e. chlorophyll) and primary production with remote sensing techniques, but is not commonly used in prognostic ecosystem modelling. Rather, as noted by Branco and Kremer (2005), Sarmiento and Gruber (2006), and Alver et al. (in press), variations in the term K_x are commonly ignored in such models (although with some exceptions, see below). Instead of using two independent measures of K_w and K_x, modellers usually assign a constant value (K_{bg}) to the background attenuation that should approximate the non-algal contribution to light absorption in the study area. In coastal waters K_{bg} might contribute much more to the total light attenuation than the phytoplankton, and salinity might serve as proxy for the background light attenuation since lower salinity generally means higher CDOM concentrations and thereby higher light attenuation (Kowalczuk et al., 2003; Branco and Kremer, 2005; Vaillancourt et al., 2005). This negative correlation between light attenuation and salinity has been utilized to represent a variable background light attenuation in some coastal and shelf ecosystem models (e.g. Walsh et al., 2003; Mei et al., 2010, see Table 1). However, constant background attenuation, in particular in ocean ecosystem models, is commonly assumed. Fasham et al. (1990) applied a K_{bg} value of 0.04 m^{-1} to represent relatively

* Corresponding author. Tel.: +47 55584478; fax: +47 55584450.
E-mail address: dag.aksnes@bio.uib.no (D.L. Aksnes).
[1] Present address: Marine Research Division, AZTI Foundation, Txatxarramendi ugartea, z/g 48395, Sukarrieta, Bizkaia, Spain.
[2] Present address: Institute of Marine Research, P.O. Box 1870, Nordnes, 5817 Bergen, Norway.

0304-3800/$ – see front matter © 2013 Elsevier B.V. All rights reserved.
http://dx.doi.org/10.1016/j.ecolmodel.2013.02.010

Table 1
Representation of background light attenuation due to water (K_w, m^{-1}) and other substances (K_x, m^{-1}) in some marine ecosystem models. In addition to the background attenuation all cited models contain a dynamic representation where simulated phytoplankton concentration contributes to the attenuation of light.

Authors	Simulated area	K_w	K_x
Fasham et al. (1990)	Station S near Bermuda	0.04	–
Aksnes and Lie (1990)	Norwegian fjord	0.04	0.1
Walsh et al. (2003)	Florida shelf	0.04[a]	$K_x = 3.470 - 0.095S$; $S > 28$ $= 0.892 - 0.003S$; $24 < S < 28$ $= 2.250 - 0.060S$; $S < 24$
Schmittner et al. (2005)	Global ocean	0.04	–
Huisman et al. (2006)	Oligotrophic ocean	0.045	–
Schrum et al. (2006)	North Sea	0.05	–
Follows et al. (2007)	Global ocean	0.04	–
Mei et al. (2010)	Gulf of St. Lawrence	0.08[b]	$K_x = 0.5325 - 0.01392S$; $S < 27$ $= 0.9823 - 0.02995S$; $S > 27$

[a] The K_w and K_x values of Walsh et al. (2003) were specified for the wavelength 443 nm while the other studies represent attenuation of PAR.
[b] The K_w value of Mei et al. (2010) was assumed to contain attenuation due to pure water in addition to substances other than CDOM and phytoplankton.

clear oceanic waters near Bermuda, and values close to this are frequently applied as background attenuation in ecosystem modelling (Sarmiento and Gruber, 2006, see also Table 1). Fasham et al. (1990) noted, however, that the background attenuation was one of the most critical parameters in their model even though it was varied on a relatively narrow range of 0.038–0.051 m^{-1}.

CDOM is a complex group of compounds that are formed by microbial degradation of organic matter of both terrestrial and marine origin. The highest concentrations are found in coastal environments such as estuaries that receive freshwater containing terrestrial CDOM. CDOM has long been known to be an important component of the optical properties, not only of coastal and estuarine environments, but also of the oceanic environment (Kirk, 2011; Morel et al., 2007; Siegel et al., 2002). Siegel et al. (2002) found that coloured detrital and dissolved materials (of which CDOM was the largest fraction) contributed equally with phytoplankton to blue light absorption at the global scale. Thus CDOM appears to play a major role in determining the light available, not only in coastal waters, but also in the open ocean (Nelson and Siegel, 2002). Increased supplies of terrestrial CDOM to lake and stream waters across much of Europe and North American have been reported during the last 30 years (Porcal et al., 2009), and further raise in CDOM is expected in regions with climate warming and increased precipitation (Larsen et al., 2011). Thus CDOM variations are likely to receive more attention in the future both as carbon sink and light attenuator. The objective of the present study is to explore how natural variations in CDOM, through its effect on the light attenuation, affect simulated euphotic zone properties in marine ecosystem models.

2. Methods

2.1. Simulation model

We have applied the general simulation model of Huisman et al. (2006). This model contains basic features that are common to most vertically resolved marine ecosystem models that have been proposed since the 1970s (e.g. Radach and Maier-Reimer, 1975; Platt et al., 1977). The model is described in Huisman et al. (2006). The dynamics of the phytoplankton population (P, cells m^{-3}) and the nutrient concentration are given by two equations (Huisman et al., 2006):

$$\frac{\partial P}{\partial t} = \mu(N,I)P - mP - v\frac{\partial P}{\partial z} + \kappa\frac{\partial^2 P}{\partial z^2} \quad (1)$$

$$\frac{\partial N}{\partial t} = -\alpha\mu(N,I)P + \varepsilon mP + \kappa\frac{\partial^2 N}{\partial z^2} \quad (2)$$

where P is the phytoplankton population density, N (mmol m^{-3}) the nutrient (nitrate) concentration, m is the specific loss rate of the phytoplankton, v is the phytoplankton sinking velocity, κ is the vertical turbulent diffusivity, α is the nitrigen content of the phytoplankton, ε is the proportion of nitrogen in dead phytoplankton that is recycled, and $\mu(N,I)$ is the specific growth rate of the phytoplankton as an increasing saturating function of nitrate availability N and light intensity I (PAR):

$$\mu(N,I) = \mu_{\max} \quad \min\left(\frac{I}{H_i + I}, \frac{N}{H_n + N}\right) \quad (3)$$

where $\mu_{\max}$ is the maximum specific growth rate of phytoplankton and H_i and H_n are the half saturation coefficient for light and nitrate respectively (symbols are summarized in Table 2).

Light intensity (I) decreases exponentially with depth:

$$I = I_{in} \quad \exp\left(-K_{bg}z - k_p\int_0^z P(t,\sigma)d\sigma\right) \quad (4)$$

where I_{in} is the incident light intensity, K_{bg} (m^{-1}) is the background light attenuation of the water column, k_p (m^2 $cell^{-1}$) is the specific light attenuation coefficient of phytoplankton cells, and σ is an integration variable accounting for the non-uniform phytoplankton population density distribution with depth. The specific light attenuation coefficient, k_p, is subject to substantial variation in nature (Bricaud et al., 1995) that is not accounted for in our analysis.

Simulated primary production and associated euphotic zone properties are severely affected by nutrient input associated with vertical mixing (e.g. Denman and Gargett, 1983; Huisman et al., 1999; Zakardjian and Prieur, 1994; Huisman et al., 2006). The effects of mixing are not emphasized in the present study, but we have mapped the effects of variation in CDOM light attenuation at three different levels of turbulent diffusivities (see below).

2.2. Parameter values

Except for the background light attenuation and the turbulent diffusivity, we apply the same parameter values (see Table 2) as in Huisman et al. (2006). Huisman et al. (2006) demonstrated that low levels of mixing, i.e. a turbulent diffusivity coefficient below 0.5×10^{-4} m^2 s^{-1}, generated oscillations and chaos in the simulated deep chlorophyll maximum (DCM). For values above this threshold they found that the phytoplankton population converged towards a stable equilibrium at which the downward flux of consumed nutrients equals the upward flux of new nitrate. We map the effects of changes in the background attenuation at three levels of turbulent diffusivities; 0.6×10^{-4} (low), 1.7×10^{-4} (medium), and 3.4×10^{-4} m^2 s^{-1} (high). The low level is just above the "chaos" threshold of 0.5×10^{-4} m^2 s^{-}, the medium level corresponds to the

Table 2
Parameter values used in the simulations. These are the same as in Huisman et al. (2006) (column A) except for the values given in column B.

Symbol	Explanation	Units	Values	
			A	B
t	Time	s		
z	Depth	m		
N	Nutrient concentration	mmol nutrient m^{-3}		
P	Phytoplankton concentration	cells m^{-3}		
I	Light intensity	μmol photons m^{-2} s^{-1}		
I_{in}	Incident light intensity	μmol photons m^{-2} s^{-1}	600	
K_{bg}	Background attenuation	m^{-1}	0.045	0.03–0.2
k_p	Specific attenuation coefficient of phytoplankton cells	m^2 $cell^{-1}$	6×10^{-10}	
z_B	Depth of the water column	m	300	1000
κ	Vertical turbulent diffusivity	m^{-2} s^{-1}	1.2×10^{-5}	$0.6–3.4 \times 10^{-4}$
μ_{max}	Maximum specific growth rate	s^{-1}	1.1×10^{-5}	
H_I	Half-saturation constant of light limited growth	μmol photons m^{-2} s^{-1}	20	
H_N	Half-saturation constant of nutrient limited growth	mmol nutrient m^{-3}	0.025	
m	Specific loss rate	s^{-1}	2.8×10^{-6}	
α	Nutrient content of phytoplankton	mmol nutrient $cell^{-1}$	1.0×10^{-9}	
ε	Nutrient recycling coefficient		0.5	
v	Sinking velocity	m s^{-1}	1.17×10^{-5}	
N_B	Nutrient concentration at z_B	mmol nutrient m^{-3}	10	

average mixing coefficient for the oceanic thermocline that was reported by Li et al. (1984), and the high level is twice this value.

We define K_{bg} as the sum of the attenuation of pure water and CDOM, and vary K_{bg} on the range 0.03–0.2 m^{-1}. According to observations reported in Morel et al. (2007) and Kirk (2011) the pure water value of 0.04 m^{-1}, which has been widely adopted in ecosystem modelling (Table 1), appears too high to represent the clearest oceanic water, and we therefore use 0.03 m^{-1} to represent pure water. The upper value of 0.2 m^{-1} corresponds to light attenuation at salinity around 25 in the Gulf of St. Lawrence (Mei et al., 2010, see Table 1). Thus our simulated scenarios correspond to a gradient from very clear oceanic water to relatively clear coastal water. CDOM attenuations much higher than 0.2 m^{-1} are found in many estuaries and other coastal environments (Kirk, 2011), but are not simulated in our study.

2.3. Numerical solution

The General Ocean Turbulence Model (GOTM) software (http://www.gotm.net/) was adapted to solve Eqs. (1) and (2). At the surface boundary it was assumed zero-fluxes of phytoplankton and nutrients and also for the phytoplankton at the bottom boundary. Nitrate, however, was replenished from below with a fixed concentration, N_B, in the deepest cell of the water column.

In GOTM the numerical solution is split into two parts, namely transport and reaction. To solve advection we used the PDM-limited P2 advection scheme that is the most accurate scheme among those available (Leonard, 1991). To solve the ordinary differential equation (ODE) of the reaction part (source and sink) we used the first order Euler (Burchard et al., 2006).

Simulations were made for a 1000 m deep water column with 1 m resolution and a time step of 300 s. The simulation experiments were initialized with a nitrate concentration of 9.9 mmol N m^{-3} and a phytoplankton concentration of 10^8 cells m^{-3} throughout the water column. A constant incident light intensity (Table 2) was applied and the simulations were run for a period that corresponded to 20 years in simulated time. This runtime ensured that the solution converged towards a euphotic zone depth so that the annual change was less than 1% per year (Fig. 1) in all simulations.

3. Results

3.1. Phytoplankton and nutrient distributions

At the lowest CDOM attenuation (K_{bg} = 0.03 m^{-1}), which corresponds to that of clear oceanic water, the depth of the DCM (taken as the depth of the maximum phytoplankton abundance) is located at 132 m at the lowest turbulent diffusivity (Fig. 2A). It shoals to 18 m depth when CDOM attenuation is raised to that representing coastal water (K_{bg} = 0.20 m^{-1}) (Fig. 2B). Another effect of this elevated CDOM attenuation is a larger DCM peak (Fig. 2).

When the turbulent diffusivity is raised from low (Fig. 2A) to high (Fig. 2C), the DCM depth shoals from 137 to 97 m for the clear oceanic water. This shoaling is, like the CDOM associated shoaling, also accompanied with a larger DCM peak (Fig. 2). Over the selected ranges of CDOM attenuation and turbulent diffusivity, the DCM depth is 2–3 times more sensitive to a change in the background attenuation than to the same relative change in the turbulent diffusivity (Table 3).

If nutricline depth is defined as the first depth with a relatively low nitrate concentration, e.g. 0.05 mmol m^{-3} (Cermeno et al., 2008), the nutricline depth is located deeper at the low (Fig. 2A and B) than at the high (Fig. 2C and D) turbulent diffusivity. However, if the nutricline depth is defined as the first depth with an intermediate nitrate concentration, e.g. 2 mmol m^{-3}, the nutricline depth is located deeper at high than at low turbulent diffusivity (Fig. 2). Thus whether the nutricline depth shoals or deepens with increased turbulent diffusivity depends on how we define nutricline depth, and this has implications for how to interpret nutricline depth as proxy for primary production (see Section 4). The overall effect of

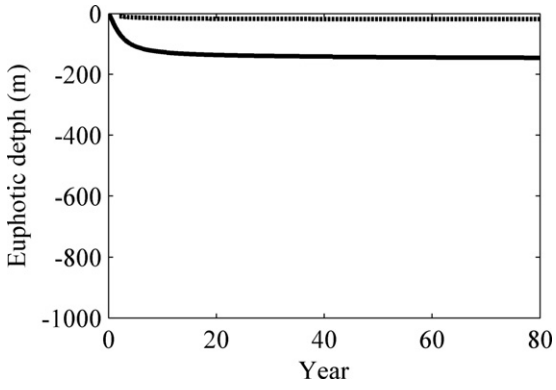

Fig. 1. Simulated euphotic depth (the depth at which 1% of the surface light penetrates) of a 1000 m water column. After 20 years, the annual change in euphotic depth was less than 1% in all simulations. Solid line represents the simulation with the lowest background light attenuation (K_{bg} = 0.03 m^{-1}) and the lowest turbulent diffusivity (0.6×10^{-4} m^{-2} s^{-1}) while the dotted line represents the simulation with the highest background light attenuation (K_{bg} = 0.20 m^{-1}) and the highest turbulent diffusivity (3.4×10^{-4} m^{-2} s^{-1}).

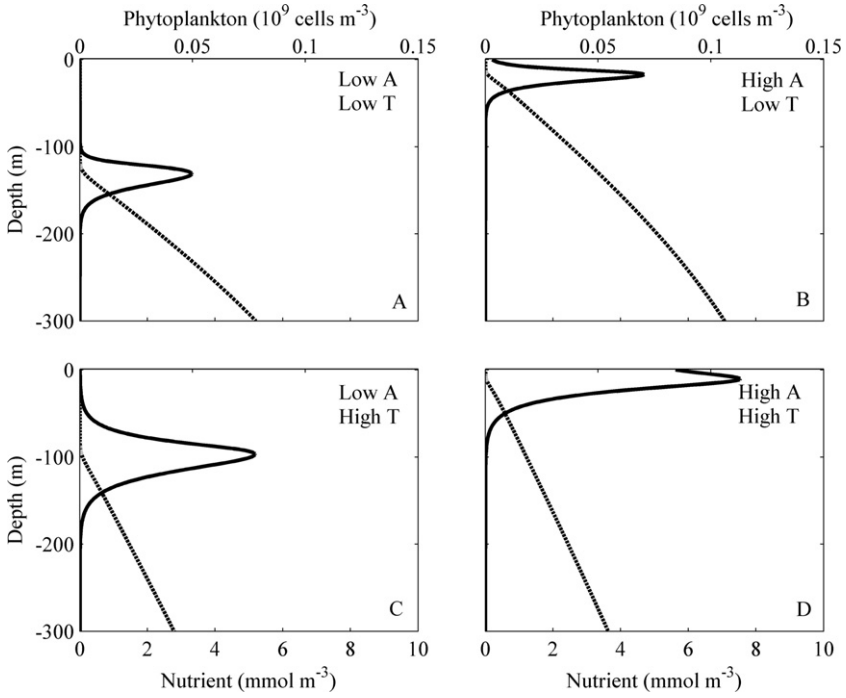

Fig. 2. Distributions of phytoplankton (solid line) and nitrate (dotted line) for combinations of low (A and C) and high (B and D) background light attenuation (K_{bg}), and low (A and B) and high (C and D) turbulent diffusivity (κ). Low A: $K_{bg} = 0.03\ m^{-1}$, High A: $K_{bg} = 0.2\ m^{-1}$, Low T: $\kappa = 0.6 \times 10^{-4}\ m^{-2}\ s^{-1}$ and High T: $\kappa = 3.4 \times 10^{-4}\ m^{-2}\ s^{-1}$.

Table 3
Sensitivity of the DCM depth, i.e. the depth (m) where the simulated phytoplankton abundance is maximal, to changes in the background attenuation and in the turbulent diffusivity. The sensitivity (S) was calculated as the relative change in the DCM depth divided by the relative change in the K_{bg}, or in κ, (Jørgensen, 1986); $S = [(y_h - y_l)/y_l]/[(x_h - x_l)/x_l]$ where x_l and x_h are the lowest ($0.03\ m^{-1}$) and highest ($0.2\ m^{-1}$) values of K_{bg} (or of κ) respectively, and y_l and y_h are the corresponding simulated values of the DCM depth.

Background attenuation K_{bg} (m^{-1})	Turbulent diffusivity (κ, $m^2\ s^{-1}$)			Sensitivity of the DCM depth to κ
	Low 0.6×10^{-4}	Medium 1.7×10^{-4}	High 3.4×10^{-4}	
0.03	132	115	97	−0.057
0.04	98	85	72	−0.057
0.05	78	67	56	−0.060
0.06	65	55	46	−0.063
0.10	38	32	26	−0.068
0.15	25	20	16	−0.077
0.20	18	14	11	−0.083
Sensitivity of DCM depth to K_{bg}	−0.152	−0.155	−0.156	

elevated CDOM attenuation is movement of the entire nutrient gradient upwards (e.g. Fig. 2B versus A) similar to nutrient upwelling (Aksnes et al., 2007). The overall effect of increased turbulent diffusivity, however, is erosion of the entire nutrient gradient (e.g. Fig. 2D versus B).

3.2. Euphotic zone properties

The depth of the euphotic zone, the depth at which 1% of the surface light penetrates, is a direct function of the light attenuation, which is equal to $\ln(0.01)/\bar{K}$, where $\bar{K}$ is the total light attenuation coefficient (i.e. including attenuation from phytoplankton as well as CDOM attenuation) between the surface and the euphotic depth. The euphotic habitat shoaled with about 100 m when CDOM attenuation was increased from 0.03 to $0.2\ m^{-1}$ (Fig. 3), but the total primary was unaffected (Fig. 4C). Furthermore, it is interesting to note that the euphotic zone shoaling is larger than that expected from the raise in CDOM attenuation alone. The additional euphotic shoaling is due to higher phytoplankton density (Fig 4A) caused by the compression of the euphotic zone. Thus a euphotic zone

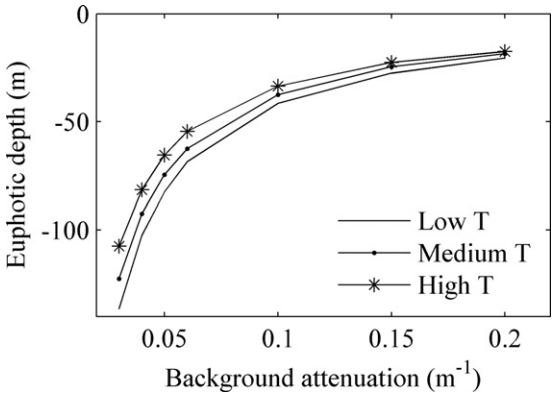

Fig. 3. The depth of the simulated euphotic zone as a function of changes in the background light attenuation at three different turbulent diffusivity levels: Low T: $\kappa = 0.6 \times 10^{-4}\ m^{-2}\ s^{-1}$, Medium T: $\kappa = 1.7 \times 10^{-4}\ m^{-2}\ s^{-1}$ and Hight T: $\kappa = 3.4 \times 10^{-4}\ m^{-2}\ s^{-1}$.

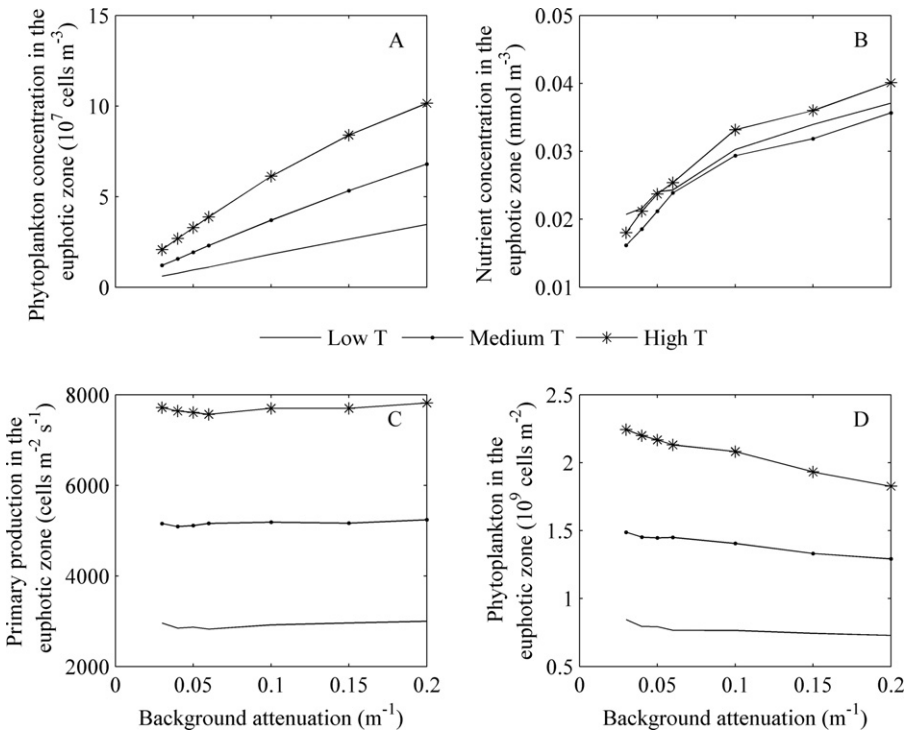

Fig. 4. Simulated euphotic zone properties as a function of changes in the background light attenuation at three different turbulent diffusivity levels: average phytoplankton (A) and nutrient (B) concentrations, total primary production (C), and total phytoplankton (D) of the euphotic zone. Low T: $\kappa = 0.6 \times 10^{-4}$ m^{-2} s^{-1}, Medium T: $\kappa = 1.7 \times 10^{-4}$ m^{-2} s^{-1} and High T: $\kappa = 3.4 \times 10^{-4}$ m^{-2} s^{-1}.

compression, initially caused by a raise in the CDOM attenuation, is further strengthened by phytoplankton crowding in a narrower habitat (Table 4). The raise in K_{bg} from 0.03 to 0.2 m^{-1} changes the total euphotic zone light attenuation, $\bar{K}$, from 0.037 to 0.241 m^{-1}. This means that the attenuation caused by the crowding of the phytoplankton cells in the euphotic zone has increased from 0.007 to 0.041 m^{-1} (Table 4). Not only the phytoplankton, but also the average nutrient concentration of the euphotic zone gets higher with increased CDOM attenuation (Fig. 4B).

Higher euphotic phytoplankton concentration is also seen in cases where turbulent diffusivity is increased (Fig. 4A), but where CDOM attenuation is invariant. In this case, however, the elevated phytoplankton concentration is primarily associated with a higher primary production (Fig. 4C) giving rise to more phytoplankton (Fig. 4D). Also for increased turbulent diffusivity the euphotic zone becomes compressed, but over the range of turbulent diffusivities applied here, this compression is not very pronounced (Fig. 3).

Table 4
The total attenuation ($\bar{K}$) of irradiance between surface and the euphotic depth increases more than the rise in the background attenuation. This is due to a narrower euphotic zone and crowding of phytoplankton (see text). The attenuation of phytoplankton in the euphotic zone represents the difference between the total attenuation and the background attenuation. The turbulent diffusivity level was intermediate (1.7×10^{-4} m^2 s^{-1}) for all simulations.

Background attenuation (K_{bg}, m^{-1})	Total attenuation ($\bar{K}$, m^{-1})	Attenuation of phytoplankton (m^{-1})
0.03	0.037	0.007
0.04	0.049	0.009
0.05	0.061	0.011
0.06	0.074	0.014
0.10	0.122	0.022
0.15	0.182	0.032
0.20	0.241	0.041

4. Discussion

Results of our simulations suggest that the vertical structure of nutrients and phytoplankton are highly sensitive to variations in CDOM attenuation, and that such variations cause changes in the vertical structure of nutrients and phytoplankton that might be confounded with changes in nutrient input (i.e. turbulent diffusivity). As discussed by Huisman et al. (1999) phytoplankton form blooms by two different mechanisms. The first mechanism corresponds to the classical Sverdrup's critical depth concept. Here a well-mixed upper layer, which is located above a pycnocline, must be shallower than a critical depth that is determined by the water column light attenuation and the phytoplankton growth affinity for light (Sverdrup, 1953). The second mechanism for bloom formation, which underlies our simulations, does not explicitly assume density stratification in any part of the water column, but requires that the turbulent diffusivity of the water column is below a critical value. The three diffusivity levels that we have used are below this value. However, we have not looked into the effects of changing the background attenuation in the Sverdrup mixed layer situation. This was addressed in Mellard et al. (2011), who also found that an increase in the background light attenuation causes an upward shift of the euphotic zone and of the phytoplankton. In nature, but also in 3D simulation models, advection, upwelling and downwelling bring additional complexity that is not resolved by our approach. Our simplified situation, however, makes it possible to analyze the sole effect of increased CDOM attenuation, but without taking into account any other natural factors that might interact and possibly override the effect of CDOM attenuation.

4.1. Nutricline depth as proxy for primary production.

One concern related to global warming is the increment of vertical density stratification of the oceans. Proposed effects of stronger

thermal stratification are decreased turbulent diffusivity, deepening of the nutricline depth (Cermeno et al., 2008; Williams and Grottoli, 2010), reduction of the nutrient flux in the euphotic zone and of the primary production (Boyce et al., 2010; Denman and Gargett, 1983; Sarmiento et al., 2004). Such patterns are studied by the use of nutricline depth as proxy for nutrient supply and primary production (e.g. Cermeno et al., 2008; Williams and Grottoli, 2010), i.e. a shallow nutricline indicates high nutrient flux, due to high turbulent diffusivity, and thereby high primary production. Our results suggest that this proxy relationship might be affected by variations in CDOM attenuation. This implies that the accuracy of the nutricline depth – primary production proxy relationship can be improved by including the effect of CDOM attenuation. Analytical models of the nutricline, which include the effect of background attenuation as well as the vertical nutrient flux (Lewis et al., 1986; Aksnes et al., 2007; Aksnes and Ohman, 2009), can be applied for this purpose.

4.2. Variations in CDOM attenuation interfere with effects of eutrophication

Our results suggest that effects of elevated CDOM attenuation resemble effects that are commonly associated with nutrient loads and eutrophication (Nixon, 1995) such as higher phytoplankton concentration, reduced visibility, and higher nutrient concentrations in the upper water column. The first part of this mechanism is straightforward. Elevated CDOM attenuation increases the light limitation at depth so that the phytoplankton, but also the nutrients (due to reduced consumption), is effectively "lifted" towards the surface. The second part involves the associated euphotic zone compression and higher phytoplankton density (Table 4). These optical effects have also been seen in models set up to simulate water columns with a mixed upper layer (Mellard et al., 2011) and upwelling (Aksnes and Ohman, 2009). Supply of terrestrial CDOM (Porcal et al., 2009; Larsen et al., 2011) to coastal waters is, according to our sensitivity analysis, likely to cause eutrophication symptoms also in cases where nutrient flux and total primary production remain unchanged. Although these symptoms might be considered as "false" eutrophication, they might be equal to effects of true eutrophication. We might also speculate that CDOM initiated shoaling and narrowing of the euphotic zone might reduce the vertical extension of e.g. the benthic macroalgae vegetation (e.g. kelp forests) with consequences for a large number of organisms and, in general, for the biodiversity that depends upon this habitat.

4.3. Knowledge of variations in CDOM attenuation might constrain uncertainty in models

The high sensitivity of the euphotic zone properties to changes in CDOM attenuation has important implications for ecosystem modelling. This appears to be particularly true for regions with a large span in CDOM attenuation such as observed along transects from oceanic to coastal waters, but also across ocean basins (Table 5). If such variation is not accounted for, this likely introduces significant errors in the way underwater light intensity is simulated. In cases where models are calibrated against observations, the resulting lack of fit might between model output and observations might then be compensated with adjustments in other processes than the light representation. This implies increased risk of compensating one error with the introduction of another error.

Efforts are currently made to include more advanced bio-optical models in traditional ecosystem models including wavelength resolution as well as effects of CDOM (e.g. Alver et al., in press and references therein). Such advanced approaches are challenged by the limited knowledge of the relationships that connect the inherent optical properties, absorption and scattering, to wavelengths and to the many particles and solvents affecting them. Before such models can be supported by data, the simpler PAR approximations, which make use of observed CDOM attenuations and/or salinity proxies (e.g. Walsh et al., 2003; Mei et al., 2010), represent a valuable option.

Table 5
Values of the light absorption coefficient (at 440 nm) in a coastal system that is exemplified by a gradient from the North Sea to increasingly more brackish water in the Baltic Sea (Table 32 in Kirk, 2011). Values are also given for the three major ocean basins where the spans represent the latitudinal variation from 80°S to 80°N in the Atlantic and in the Pacific Basins and from 80°S to 20°N for the Indian Bain (from Fig. 3 in Siegel et al., 2002). The values reported in Kirk (2011 refers to CDOM absorption, while the values reported in Siegel et al. (2002) is the absorption due to coloured detrital and dissolved materials (CDM).

Coastal system	$a(440)\,(m^{-1})$	Ocean basins	$a(440)\,(m^{-1})$
North sea	0.03–0.06	Atlantic	0.006–0.08
Skagerrak	0.05–0.12	Pacific	0.005–0.10
Kattegat	0.12–0.27	Indian	0.007–0.10
Baltic sea	0.26–0.42		

In conclusion, our results suggest that the simulated euphotic zone properties are quite sensitive to variations in CDOM attenuation that are known to occur in oceanic and coastal waters. Hence, knowledge of CDOM variation should be utilized in marine ecosystem modelling, but also in analyses where nutricline depth is applied as proxy for primary production. Finally, coastal areas (that are likely to experience increased loads of terrestrial CDOM) are expected to show optically induced eutrophication symptoms.

Acknowledgement

This study was financially supported from the Norwegian Research Council (Project nos. 196444/S40 and 190665/V40).

References

Aksnes, D.L., Lie, U., 1990. A coupled physical biological pealgic model of a shallow sill fjord. Estuarine Coastal and Shelf Science 31, 459–486.
Aksnes, D.L., Ohman, M.D., 2009. Multi-decadal shoaling of the euphotic zone in the southern sector of the California CurrentSystem. Limnology and Oceanography 54, 1272–1281.
Aksnes, D.L., Ohman, M.D., Riviere, P., 2007. Optical effect on the nitracline in a coastal upwelling area. Limnology and Oceanography 52, 1179–1187.
Alver, M.O., Hancke, K., Sakshaug, E., Slagstad, D. A spectrally-resolved light propagation model for aquatic systems: steps toward parameterizing primary production, Journal of Marine Systems, http://dx.doi.org/10.1016/j.jmarsys.2012.03.007, in press.
Boyce, D.G., Lewis, M.R., Worm, B., 2010. Global phytoplankton decline over the past century. Nature 466, 591–596.
Branco, A.B., Kremer, J.N., 2005. The relative importance of chlorophyll and colored dissolved organic matter (CDOM) to the prediction of the diffuse attenuation coefficient in shallow estuaries. Estuaries 28, 643–652.
Bricaud, A., Stramski, D., 1990. Spectral absorption coefficients of living phytoplankton and nonalgal biogenous matter: a comparison between the Peru upwelling area and the Saragasso Sea. Limnology and Oceanography 35, 562–582.
Bricaud, A., Babin, M., Morel, A., Claustre, H., 1995. Variability in the chlorophyll-specific absorption-ciefficients of natural phytoplankton: analysis and parameterization. Journal of Geophysical Research-Oceans 100, 13321–13332.
Burchard, H., Bolding, K., Kühn, W., Meister, A., Neumann, T., Umlauf, L., 2006. Description of a flexible and extendable physical-biogeochemical model system for the water column. Journal of Marine Systems 61, 180–211.
Cermeno, P., Dutkiewicz, S., Harris, R.P., Follows, M., Schofield, O., Falkowski, P.G., 2008. The role of nutricline depth in regulating the ocean carbon cycle. Proceedings of the National Academy of Science 105, 20344–20349.
Denman, K.L., Gargett, A.E., 1983. Time and space scales of vertical mixing and advection of phytoplankton in the upper ocean. Limnology and Oceanography 28, 801–815.
Fasham, M.J.R, Ducklow, H.W., Mckelvie, S.V., 1990. A nitrogen-based model of plankton dynamics in the oceanic mixed layer. Journal of Marine Research 48, 591–639.
Follows, M.J., Dutkiewicz, S., Grant, S., Chisholm, S.W., 2007. Emergent biogeography of microbial communities in a model ocean. Science 315, 1843–1846.
Huisman, J., Pham Thi, N.N., Karl, D.M., Sommeijer, B., 2006. Reduced mixing generates oscillations and chaos in the oceanic deep chlorophyll maximum. Nature 439, 322–325.

Huisman, J., Van Oostveen, P., Weissing, F.J., 1999. Critical depth and critical turbulence: two different mechanisms for the development of phytoplankton blooms. Limnology and Oceanography 44, 1781–1787.
Jørgensen, S.E., 1986. Fundamentals of Ecological Modelling. Developments in Environmental Modelling 9. Elsevier, Amsterdam.
Kirk, J.T.O., 2011. Light and Photosynthesis in Aquatic Ecosystems. Cambridge University Press, Cambridge.
Kowalczuk, P., Cooper, W., Whitehead, R., Durako, M., Sheldon, W., 2003. Characterization of CDOM in an organic-rich river and surrounding coastal ocean in the South Atlantic Bight. Aquatic Sciences 65, 384–401.
Larsen, S., Andersen, T., Hessen, D.O., 2011. Climate change predicted to cause severe increase of organic carbon in lakes. Global Change Biology 17, 1186–1192.
Leonard, B.P., 1991. The ultimate conservative difference scheme applied to unsteady one dimensional advection. Computer Methods in Applied Mechanics and Engineering 88, 17–74.
Lewis, M.R., Harrison, W.G., Oakey, N.S., Herbert, D., Platt, T., 1986. Vertical nitrate fluxes in the oligotrophic ocean. Science 234, 870–873.
Li, Y.H., Peng, T.H., Broecker, W.S., Ostlund, H.G., 1984. The average vertical mixing coefficient for the oceanic thermocline. Tellus Series B: Chemical and Physical Meteorology 36, 212–217.
Mei, Z.P., Saucier, F.J., Le Fouest, V., Zakardjian, B., Sennville, S., Xie, H.X., Starr, M., 2010. Modeling the timing of spring phytoplankton bloom and biological production of the Gulf of St. Lawrence (Canada): effects of colored dissolved organic matter and temperature. Continental Shelf Research 30, 2027–2042.
Morel, A., Gentili, B., Claustre, H., Babin, M., Bricaud, A., Ras, J., Tieche, F., 2007. Optical properties of the "clearest" natural waters. Limnology and Oceanography 52, 217–229.
Mellard, J.P., Yoshiyama, K., Litchman, E., Klausmeier, C.A., 2011. The vertical distribution of phytoplankton in stratified water columns. Journal of Theoretical Biology 269, 16–30.
Nelson, N.B., Siegel, D.A., 2002. Chromophoric DOM in open ocean. In: Hansell, D.A., Carslon, C.A. (Eds.), Biochemistry of Marine Dissolved Organic Matter. Academic Press, pp. 547–573.
Nixon, S.W., 1995. Coastal marine eutrophication: a definition, social causes, and future concerns. Ophelia 41, 199–219.
Platt, T., Denman, K.L., Jassby, A.D., 1977. Modeling the productivity of phytoplankton. In: Goldberg, E.D. (Ed.), The Sea: Ideas and observations on progress in the study of the seas, vol. VI. John Wiley, New York, pp. 807–856.
Porcal, P., Koprivnjak, J.F., Molot, L.A., Dillon, P.J., 2009. Humic substances-part 7: the biogeochemistry of dissolved organic carbon and its interactions with climate change. Environmental Science and Pollution Research 16, 714–726.
Radach, G., Maier-Reimer, E., 1975. The vertical structure of phytoplankton growth dynamics. A mathematical model. Mémoires Société Royale des Sciences de Liège 7, 113–146.
Sarmiento, J.L., Gruber, N., 2006. Ocean Biogeochemical Dyn8amics. Princeton University Press, Princeton.
Sarmiento, J.L., Slater, R., Barber, R., Bopp, L., Doney, S.C., Hirst, A.C., Kleypas, J., Matear, R., Mikolajewicz, U., Monfray, P., Soldatov, V., Spall, S.A., Stouffer, R., 2004. Response of ocean ecosystems to climate warming. Global Biogeochemical Cycles 18, GB3003, http://dx.doi.org/10.1029/2003GB002134.
Schrum, C., Alekseeva, I., St John, M., 2006. Development of a coupled physical-biological ecosystem model ECOSMO – Part I: Model description and validation for the North Sea. Journal of Marine Systems 61, 79–99.
Schmittner, A., Oschlies, A., Giraud, X., Eby, M., Simmons, H.L., 2005. A global model of the marine ecosystem for long-term simulations: sensitivity to ocean mixing, buoyancy forcing, particle sinking, and dissolved organic matter cycling. Global Biogeochemical Cycles 19, GB3004, http://dx.doi.org/10.1029/2004GB002283.
Siegel, D.A., Maritorena, S., Nelson, N.B., Hansell, D.A., Lorenzi-Kayser, M., 2002. Global distribution and dynamics of colored dissolved and detrital organic materials. Journal of Geophysical Research 107, http://dx.doi.org/10.1029/2001JC000965, p. C12, 3228.
Sverdrup, H.U., 1953. On conditions for the vernal blooming of phytoplankton. Journal du Conseil International pour l'Exploration de la Mer 18, 287–295.
Travers, M., Shin, Y.J., Jennings, S., Cury, P., 2007. Towards end-to-end models for investigating the effects of climate and fishing in marine ecosystems. Progress in Oceanography 75, 751–770.
Vaillancourt, R.D., Marra, J., Prieto, L., Houghton, R.W., Hales, B., Hebert, D., 2005. Light absorption and scattering by particles and CDOM at the New England shelf-break front. Geochemistry, Geophysics, Geosystems 6, Q11003, http://dx.doi.org/10.1029/2005GC000999.
Walsh, J.J., Weisberg, R.H., Dieterle, D.A., He, R.Y., Darrow, B.P., Jolliff, J.K., Lester, K.M., Vargo, G.A., Kirkpatrick, G.J., Fanning, K.A., Sutton, T.T., Jochens, A.E., Biggs, D.C., Nababan, B., Hu, C.M., Muller-Karger, F.E., 2003. Phytoplankton response to intrusions of slope water on the West Florida Shelf: models and observations. Journal of Geophysical Research: Oceans 108, 1–23.
Williams, B., Grottoli, A.G., 2010. Recent shoaling of the nutricline and thermocline in the western tropical Pacific. Geophysical Research Letters 37, L22601, http://dx.doi.org/10.1029/2010gl044867.
Zakardjian, B., Prieur, L., 1994. A numerical study of primary production related to vertical turbulent diffusion with special reference to vertical motions of the phytoplankton cells in nutrient and light fields. Journal of Marine Systems 5, 267–295.